Strain-induced magnetization change in patterned ferromagnetic nickel nanostructures

Alexandre Bur, Tao Wu, Joshua Hockel, Chin-Jui Hsu, Hyungsuk K. D. Kim, Tien-Kan Chung, Kin Wong, Kang L. Wang, and Gregory P. Carman

Citation: Journal of Applied Physics **109**, 123903 (2011); doi: 10.1063/1.3592344
View online: http://dx.doi.org/10.1063/1.3592344
View Table of Contents: http://scitation.aip.org/content/aip/journal/jap/109/12?ver=pdfcov
Published by the AIP Publishing

Strain-induced magnetization change in patterned ferromagnetic nickel nanostructures

Alexandre Bur,[1] Tao Wu,[1] Joshua Hockel,[1] Chin-Jui Hsu,[1] Hyungsuk K. D. Kim,[2] Tien-Kan Chung,[3] Kin Wong,[4] Kang L. Wang,[4] and Gregory P. Carman[1]
[1]*Department of Mechanical and Aerospace Engineering, University of California, Los Angeles, California 90095, USA*
[2]*Department of Materials Science and Engineering, University of California, Los Angeles, California 90095, USA*
[3]*Department of Mechanical Engineering, National Chiao Tung University, Hsinchu, Taiwan 300*
[4]*Department of Electrical Engineering, University of California, Los Angeles, California 90095, USA*

(Received 6 March 2011; accepted 14 April 2011; published online 17 June 2011)

We report strain-induced coercive field changes in patterned $300 \times 100 \times 35$ nm^3 Ni nanostructures deposited on Si/SiO_2 substrate using the magnetoelastic effect. The coercive field values change as a function of the applied anisotropy strain ($\sim$1000 ppm) between 390 and 500 Oe, demonstrating that it is possible to gradually change the coercive field elastically. While the measured changes in coercive field cannot be accurately predicted with simple analytical predictions, fairly good agreement is obtained by using a micromagnetic simulation taking into account the influence of nonuniform strain distribution in the Ni nanostructures. The micromagnetic simulation includes a position dependant strain-induced magnetic anisotropy term that is computed from a finite element mechanical analysis. Therefore, this study experimentally corroborates the requirement to incorporate mechanical analysis into micromagnetic simulation for accurately predicting magnetoelastic effects in patterned ferromagnetic nanostructures. © *2011 American Institute of Physics*. [doi:10.1063/1.3592344]

I. INTRODUCTION

In the context of magnetic recording technologies, patterned ferromagnetic nanostructures relying on conventional integrated circuit fabrication have been extensively investigated.[1] Patterning nanostructures into elongated shapes typically provide two stable magnetization states that are suitable for storing bit information. One of the most important characteristics of the structure is the magnetic coercive field, a parameter characterizing the energy barrier required to switch the magnetization between two stable states. The coercive field is a function of geometric parameters (e.g., shape, aspect ratio, and miniaturization) as well as material parameters (e.g., magnetocrystalline anisotropy and crystal structure) and these have been widely investigated experimentally[1–3] and theoretically with micromagnetic simulations.[4–7] However, a detailed investigation of controlling the coercive field using magnetoelastic effects on patterned nanostructures is relatively absent in the literature. Furthermore, the correlation between experimental results and simulations has not been adequately performed, and this is required for designing structures for specific applications with a high degree of confidence.

In the context of magnetic random access memory[8,9] (MRAM), controlling the coercive field during operation is an attractive technique to resolve both the writing energy and selectivity issues in the magnetic field driven MRAM technology. First, decreasing the energy barrier reduces the writing current required to switch the magnetization. Second, decreasing the energy barrier during writing while maintaining a large energy barrier in neighboring ferromagnetic units, provides a higher switching reliability, and eliminates erroneous switching of half-selected units. One approach that has not been studied extensively is to elastically control the magnetic coercive field by changing the internal strain state of the ferromagnetic unit. In practice, this can be achieved by using a ferroelectric layer to electrically control the strain states of the ferromagnetic unit, i.e., converse magnetoelectric effect[10] (CME). The CME has been widely investigated in bulk and to a lesser degree in thin film ferromagnetic materials;[11–13] however, very few studies exist on patterned nanostructures. Chung *et al.*[14] reported qualitative experimental data on electrically induced magnetization changes in Ni rectangular nanostructures deposited onto a PZT film. Zavaliche *et al.*[15] experimentally investigated magnetization reversal in ferrimagnetic $CoFe_2O_4$ vertical nano-pillars embedded in ferroelectric $BiFeO_3$ and highlighted the advantage of using the CME effect during magnetization reversal in systems with perpendicular magnetic anisotropy. However, none of these studies directly correlate the electrically-induced strain to the coercive field changes on the nanostructures. While a few studies exist on CME and nanostructures, a study comparing experimental data with predictions from micromagnetic models is still absent in the literature.

In this article, we quantify the strain-induced coercive field changes in patterned Ni nanostructures ($L_y = 300$, $L_x = 100$, and $L_z = 35$ nm) deposited onto a Si/SiO_2 substrate. Strain is applied to the nanostructures using a four point bending setup[16] and magnetization curves (M-H) are measured by Magneto-Optical Kerr Effect (MOKE) magnetometry for different strain states. This experimental study demonstrates that it is possible to gradually change the coercive field by externally applying anisotropic strain to the patterned nanostructures. In addition, these experimental results

are compared with an existing micromagnetic model originally proposed by Dean *et al.*[17] incorporating finite element mechanical analysis. Our results shows that experimental data agree with the simulation when nonuniform strain distribution is incorporated into the micromagnetic simulation using a position dependant strain-induced magnetic anisotropy term.

II. EXPERIMENT

The specimen used in this study consists of a 10×10 mm^2 Ni nanostructure array fabricated on Si/SiO_2 substrate as shown in Fig. 1(a). The 300×100 nm nanostructures are fabricated by e-beam lithography (Vistec EBPG5000+), e-beam evaporation, and lift-off process.[14] A 5 nm Ti adhesion layer and a 35 nm Ni layer are deposited onto SiO_2 using e-beam evaporation prior to lift-off. Figure 1(a) shows an SEM image of the nanostructures while Fig. 1(b) shows a magnetic force microscopy (MFM) image of the as-fabricated nanostructures. The color scale quantifies the magnetic interaction between the tip and sample. Dark and bright contrasts characterize attractive and repulsive interaction, respectively. The MFM image indicates a preferred axis of magnetization along the length of the nanostructure (i.e., y-direction), showing in-plane magnetic dipoles either oriented parallel (bright-dark contrast) or anti-parallel (dark-bright contrast) to the y-direction. Therefore, the magnetic dipoles observed from the MFM image confirm the single domain state for the considered dimensions.

The four-point bending setup used to impose anisotropic strains onto the substrate as shown in Fig. 2. In a four-point bending experiment, the strain at the top surface of the substrate is uniform between the inner bearings.[18] This method was previously used to characterize the magnetoelastic response of continuous ferromagnetic thin films.[19] The mechanical load is applied to a fiber glass layer on which the Si/SiO_2 substrate is bonded to extend the Ni nanobars further from the neutral axis to minimize stress/strain variations. Two different setups are used to apply anisotropic strains, producing two modes of strain: (1) tensile strain along x (x-direction) and compressive strain along y (y-direction) as shown in Fig. 2(a) or (2) compressive strain along x and tensile strain along y as shown in Fig. 2(b). Two strain gauges are attached to the Si/SiO_2 substrate to measure the strain values ε_{yy} and ε_{xx} experienced by the SiO_2 adjacent to the Ni

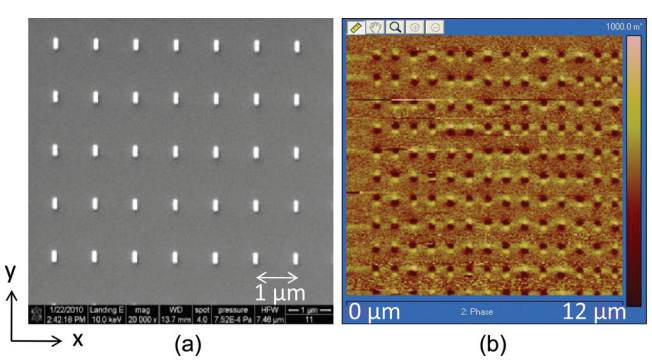

FIG. 1. (Color online) (a) SEM image and (b) MFM image of the Ni nanostructures array.

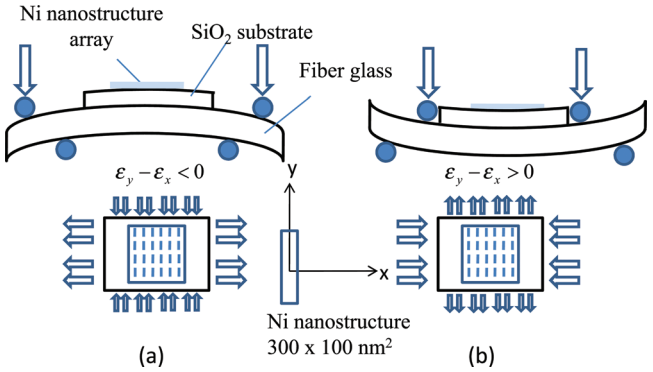

FIG. 2. (Color online) Two different setups are used to apply anisotropic strains: (a) $\varepsilon_y - \varepsilon_x < 0$ and (b) $\varepsilon_y - \varepsilon_x > 0$.

nanostructures. Magnetization curves are measured with a MOKE magnetometer as a function of the applied strain states. The MOKE measurements are performed along the y axis, i.e., the magnetization easy axis of the nanostructures.

To evaluate the spatial distribution of the strain in the Ni nanostructures, a finite element mechanical analysis was used. A single Ni nanostructure on top of a SiO_2 layer was modeled using 3-D solid elements to evaluate the strain variations both in xy plane as well as through the thickness (z direction). These nonuniform strain distributions in the Ni single domain were used as input to the micromagnetic simulations. To incorporate the spatial strain distribution results into the micromagnetic simulation, the strain computed in the mechanical analysis is converted to a strain-induced magnetoelastic anisotropy coefficient for each discretized element. This magnetoelastic anisotropy coefficient which varies from element to element is incorporated into the micromagnetic simulation. The micromagnetic simulation is a three-dimensional micromagnetic model based on the Landau-Lifshift-Gilbert equation and the results are used to estimate the coercive field changes as a function of the applied strain. The equilibrium magnetization results from the minimization of the free energy $E_{tot} = E_{dm} + E_{ex} + E_{zm} + E_{mc} + E_{me}$ including the demagnetizing E_{dm}, exchange E_{ex}, Zeeman E_{zm}, and magnetocrystalline anisotropy E_{mc} energy terms, as well as an additional magnetoelastic term E_{me} calculated from the mechanical analysis.

III. RESULT AND DISCUSSION

Figure 3 plots the experimentally measured normalized magnetization versus the applied magnetic field for different applied relative strain differences ($\varepsilon_{yy} - \varepsilon_{xx}$). The unstrained curve (indicated by black squares) shows a hysteresis curve with an initial high squareness ratio M_r/M_s and large coercive field H_c of 450 Oe due to shape anisotropy. As the relative strain ($\varepsilon_{yy} - \varepsilon_{xx}$) changes from -1210 to $+1060$ ppm, the coercive field ranges between 390 and 500 Oe. In comparison to the unstrained curve, the H_c values increase up to 11% for $\varepsilon_{yy} - \varepsilon_{xx} < 0$, while H_c decreases up to 13% for $\varepsilon_{yy} - \varepsilon_{xx} > 0$. Referred to as the Villari effect, a change in magnetic anisotropy is induced elastically when changing the strain state of a ferromagnetic material. Assuming first order terms, the magnetoelastic energy formulation $E_{me}(\alpha_i,$

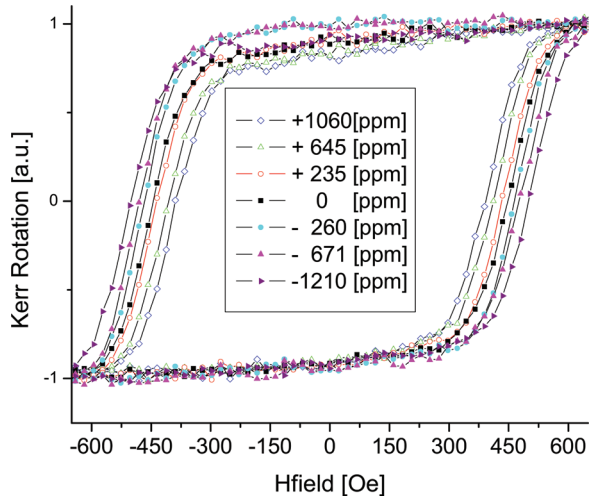

FIG. 3. (Color online) M-H curves measured along y for different relative strain difference $(\varepsilon_{yy} - \varepsilon_{xx})$.

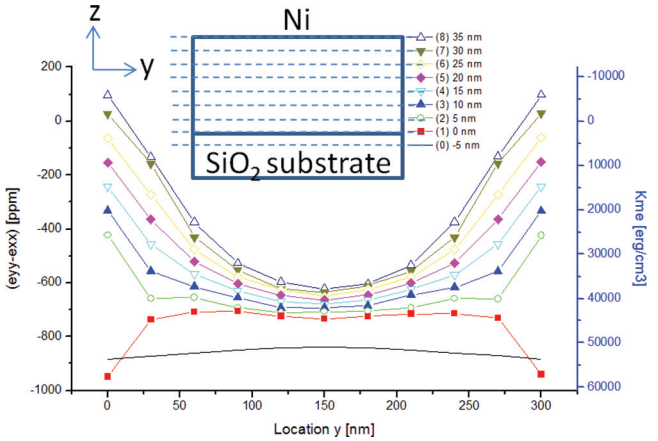

FIG. 4. (Color online) Relative strain $(\varepsilon_{yy} - \varepsilon_{xx})$ and magnetoelastic K_{me} computed from the simulation as a function of the location y. The curves represent different thicknesses.

ε_{ij}) for cubic crystal structure depends on the strain tensor matrix represented by ε_{ij} and magnetization direction represented by the cosine directions α_i with respect to the principal strain direction:

$$E_{me}(\alpha_i,\varepsilon_{ij}) = B_1\left[\varepsilon_{xx}\left(\alpha_1^2 - \frac{1}{3}\right) + \varepsilon_{yy}\left(\alpha_2^2 - \frac{1}{3}\right) + \varepsilon_{zz}\left(\alpha_3^2 - \frac{1}{3}\right)\right] + B_2\left(\varepsilon_{xy}\alpha_1\alpha_2 + \varepsilon_{yz}\alpha_2\alpha_3 + \varepsilon_{xz}\alpha_1\alpha_3\right). \quad (1)$$

$B_{1,2}$ represents the magnetoelastic coupling coefficients and depends on the magnetostriction coefficients $\lambda_{<100>}$ and $\lambda_{<111>}$, as well as the Young's modulus E of the ferromagnetic material. Below, we approximate the magnetoelastic energy for an anisotropic in-plane strain configuration, as measured in this study. Isotropic magnetostriction is assumed due to the polycrystalline structure of the Ni single domains, and the strain terms ε_{zz}, ε_{xy}, ε_{yz}, ε_{xz} are assumed negligible compared to ε_{xx} and ε_{yy}. This assumption is confirmed in the finite element mechanical analysis. As reported in previous studies,[20] the magnetoelastic energy simplifies to a uniaxial magnetic anisotropy defined as:

$$E_{me} = K_{me}\left(1 - \alpha_2^2\right), \text{where } K_{me} = \frac{3}{2}\lambda_s E\left(\varepsilon_{yy} - \varepsilon_{xx}\right). \quad (2)$$

The magnetoelastic anisotropy coefficient K_{me} is defined along the y-axis and depends on the in-plane strain difference $(\varepsilon_{yy} - \varepsilon_{xx})$ and the saturation magnetostriction λ_s. When the strain difference is negative $(\varepsilon_{yy} - \varepsilon_{xx} < 0)$, a positive anisotropy is induced along the easy axis, since Ni has negative magnetostriction. By increasing the magnetic anisotropy, the coercive field increases, as observed in the experimental results shown in Fig. 3. Similarly, when the strain difference is reversed $(\varepsilon_y - \varepsilon_x > 0)$, a negative magnetic anisotropy is induced, resulting in a decrease in the coercive field. This qualitatively describes the trends observed in Fig. 3. However, to quantify the coercive field change, a micromagnetic simulation is required to model the magnetization dynamics due to incoherent magnetization rotation in ferromagnetic single domains during magnetization reversal. We note that the classical Stoner Wohlfarth model to estimate the change in coercive field $\Delta H_c = 2\Delta K_{eff}/M_s$ as a function of the effective change in magnetic anisotropy ΔK_{eff} significantly overestimate ΔH_c due to the invalid assumption of coherent rotation during magnetization reversal.

Regarding the mechanical analysis, the strain state in the Ni single domain is computed assuming the SiO_2 substrate is perfectly bonded to the Ni single domain. The strain state in the substrate is initially defined by the anisotropic strain values measured by the strain gauges attached to the SiO_2 substrate. The Young's modulus and Poisson's ratio of Ni and SiO_2 are, respectively, $E_{Ni} = 180$ GPa, $\nu_{Ni} = 0.3$, $E_{SiO2} = 70$ GPa, and $\nu_{SiO2} = 0.2$. Figure 4 (vertical axis on the left) shows the predicted relative strain $(\varepsilon_{yy} - \varepsilon_{xx})$ in a single Ni nanostructure as a function of the y location for different z values (i.e., strain varies through the thickness). The nine different curves illustrate the strain distribution in (a) the SiO_2 substrate 5 nm below the SiO_2/Ni interface (curve 0), (b) the SiO_2/Ni interface (curve 1), and (c) different selected thicknesses in the Ni nanostructure (curves 2 to 8). The results show highly nonlinear strain profiles in the Ni single domain, demonstrating that significant strain variations occur along the y and z directions. The strain profiles show a maximum (absolute value) located in the center part and a decrease near the edges, i.e. a classical shear lag type of variation well known in the mechanics community.

Regarding the micromagnetic simulations, the volume of the rectangular single domain is uniformly discretized into 6240 cubic elements, with sampling $N_x = 20$, $N_y = 60$, $N_z = 7$ along the three principal directions. The dimension of the cubic elements is four times smaller than the exchange length to ensure accurate computation. As illustrated in Fig. 4 (vertical axis on the right), for each discretized element, a strain-induced magnetoelastic anisotropy coefficient K_{me} is computed from Eq. (2) as a function of the strain distribution defined in Fig. 4. We note that the sign of K_{me} is opposite to $(\varepsilon_{yy} - \varepsilon_{xx})$ due to negative Ni magnetostriction. Regarding numerical values used in the simulation, the magnetization saturation $M_s = 480$ erg/cm^3 and the exchange coupling

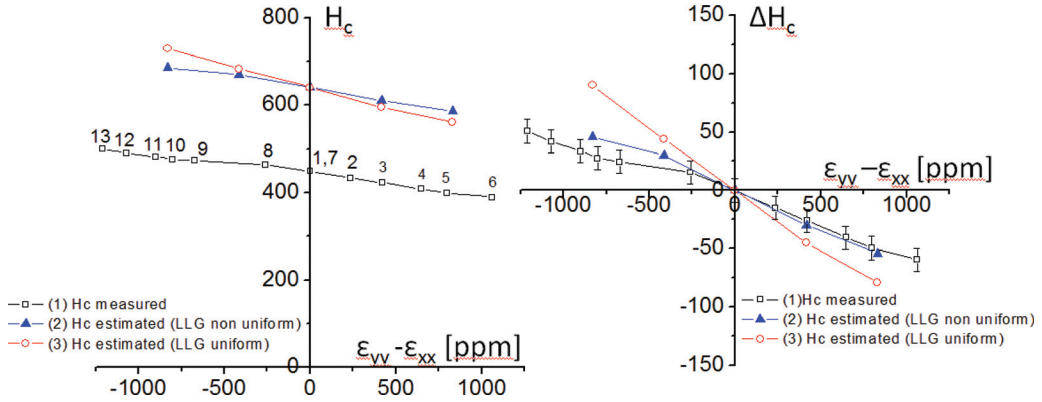

FIG. 5. (Color online) (a) Coercive field H_c and (b) strain-induced coercive field variation ΔH_c as a function of relative strain difference $(\varepsilon_y - \varepsilon_x)$. The lines are guides for the eyes.

$A = 10^{-6}$ erg/cm are defined from bulk Ni. The magnetocrystalline anisotropy constant K_1 and K_2 are set to zero, due to their relatively low values compared to other terms as well as due to the polycrystalline nature of the Ni nanostructures. The product of the Young's modulus E and magnetostriction coefficient $E \cdot \lambda_s = -4.05$ MPa have been determined experimentally from 35 nm Ni thin film using the anisotropy field variation ΔH_k method.[19] Assuming a Young's modulus E = 180 GPa, this would results in a magnetostriction coefficient $\lambda_s = -22.5$ ppm, which is in the same range to λ_s reported in bulk Ni. In our simulation, we make the assumption that there is no significant change in magnetoelastic properties (i.e., the product $E \cdot \lambda_s = -4.05$ MPa used in the simulation) between a thin film and a patterned nanostructure as soon as the continuum mechanics hypothesis is still valid for dimension in the 100 nm range.

Figure 5 shows a comparison between the experimental data (curve 1) and two different micromagnetic simulations. The two different micromagnetic models considered are: 1) a model that computes the K_{me} coefficients from the nonuniform strain distribution (curve 2) and 2) a model that computes the K_{me} coefficients from the strain gauge values measured at the SiO_2 top surface assuming uniform strain distribution within the Ni nanostructure (curve 3). Figure 5(a) and (b) show, respectively, the coercive field H_c and the change in coercive field ΔH_c as a function of the measured relative strain difference $(\varepsilon_{yy} - \varepsilon_{xx})$. The numbers located above the experimental curve indicate the sequence of the experiment. All curves indicate a linear trend between H_c and $(\varepsilon_{yy} - \varepsilon_{xx})$, which is in agreement with the magnetoelastic anisotropy formulation considering only first order terms. When comparing experimental and simulation H_c data [Fig. 5(a)], we observe a disagreement between the curves of approximately 200 Oe. This difference is attributed to geometry differences such as aspect ratio, shape, or surface roughness not taken into account in the model.[1] More importantly, when comparing the change in coercive field ΔH_c data shown in Fig. 5(b), good agreement is observed between the experimental data (curve 1) and the model assuming nonuniform strain distribution (curve 2). We note a visible discrepancy close to the error range on the left part of the graph (points 8 to 13) which may be attributed to an experimental measurement error during the strain points 8 and 9, shifting the remaining measurements (points 10 to 13) due to cumulative error. The model assuming uniform strain distribution (curve 3) clearly overestimates the experimental data by 50% which is considerably larger than the predictions using the nonuniform strain model. This discrepancy is attributed to an overestimation of the strain values in the Ni nanostructure as can be seen in Fig. 4. Therefore, the data presented in Fig. 5 confirms that fairly accurate predictive capabilities are obtained for micromagnetic simulations integrated with mechanical analysis when the nonuniform strain distribution is incorporated into the simulation.

IV. SUMMARY

In conclusion, we first demonstrated experimentally that it is possible to gradually control the coercive field of ferromagnetic single domain nanostructures by controlling the strain state and applying anisotropic strain on the order of 1000 ppm. The micromagnetic simulation is in agreement with the experimental coercive field change ΔH_c. The experimental data are in agreement with micromagnetic simulation only when modeling nonuniform strain distribution within the Ni nanostructures and including a position dependant strain-induced magnetic anisotropy term. Therefore, this study validates experimentally an existing micromagnetic model[17] applied to patterned ferromagnetic nanostructures and reveals the importance to consider the nonuniformity of the strain profile.

ACKNOWLEDGMENTS

The authors appreciate Scott Keller and Michael C. Emmons for their valuable discussions and acknowledge the use of the scanning probe microscopy facility at the Nano and Pico Characterization Laboratory at the California NanoSystems Institute. This work was supported by the U.S. ARMY RESEARCH OFFICE (ARO) under Grant No. W911NF-08-1-0125 managed by Dr. Bruce LaMattina, Air Force Office of Scientific Research (AFOSR) under Grant No. FA9550-09-1-0677 managed by Byung-Lip (Les) Lee, and the Swiss National Science Foundation (SNF) under Grant No. PBNEP2-124323.

[1] J. I. Martin, J. Nogues, K. Liu, J. L. Vicent, and I. K. Schuller, J. Magn. Magn. Mater. **256**(1–3), 449 (2003).

[2]C. A. Ross, S. Haratani, F. J. Castano, Y. Hao, M. Hwang, M. Shima, J. Y. Cheng, B. Vogeli, M. Farhoud, M. Walsh, and H. I. Smith, J. Appl. Phys. **91**(10), 6848 (2002).
[3]R. P. Cowburn, J. Appl. Phys. **93**(11), 9310 (2003).
[4]R. Ferre, Comp. Mat. Sci. **10**(1-4), 278 (1998).
[5]J. Shi, T. Zhu, M. Durlam, E. Chen, S. Tehrani, Y. F. Zheng, and J. G. Zhu, IEEE Trans. Mag. **34**(4), 997 (1998).
[6]A. Aharoni, J. Magn. Magn. Mater. **197**, 786 (1999).
[7]K. J. Kirk, M. R. Scheinfein, J. N. Chapman, S. McVitie, M. F. Gillies, B. R. Ward, and J. G. Tennant, J. Phys. D Appl. Phys. **34**(2), 160 (2001).
[8]J. G. Zhu, P IEEE **96**(11), 1786 (2008).
[9]R. L. Comstock, J. Mater. Sci. Mater. El. **13**(9), 509 (2002).
[10]T. Wu, C.-M. Chang, T.-K. Chung, and G. P. Carman, IEEE Trans. Magn. **45**(10), 4333 (2009).
[11]C.-W. Nan, M. I. Bichurin, S. X. Dong, D. Viehland, and G. Srinivasan, J. Appl. Phys. **103**(3), 031101 (2008).
[12]T. Wu, M. Emmons, T.-K. Chung, J. Sorge, and G. P. Carman, J. Appl. Phys. **107**(9), 09D912 (2010).
[13]Y. M. Jia, S. W. Or, H. L. W. Chan, X. Y. Zhao, and H. S. Luo, Appl. Phys. Lett. **88**(24), 242902 (2006).
[14]T.-K. Chung, S. Keller, and G. P. Carman, Appl. Phys. Lett. **94**(13), 132501 (2009).
[15]F. Zavaliche, T. Zhao, H. Zheng, F. Straub, M. P. Cruz, P. L. Yang, D. Hao, and R. Ramesh, Nano. Lett. **7**(6), 1586 (2007).
[16]T. Wu, A. Bur, J. L. Hockel, K. Wong, T.-K. Chung, and G. P. Carman, IEEE Magn. **2**, 6000104 (2011).
[17]J. Dean, M. T. Bryan, G. Hrkac, A. Goncharov, C. L. Freeman, M. A. Bashir, T. Schrefl, and D. A. Allwood, J. Appl. Phys. **108**(7), 073903 (2010).
[18]V. Weihnacht, W. Bruckner, and C. M. Schneider, Rev. Sci. Instrum. **71**(12), 4479 (2000).
[19]R. C. O'Handley, O.-S. Song, and C. A. Ballentine, J. Appl. Phys. **74**(10), 6302 (1993).
[20]M. Weiler, A. Brandlmaier, S. Geprägs, M. Althammer, M. Opel, C. Bihler, H. Huebl, M. S. Brandt, R. Gross and S. T. B. Goennenwein, New J. Phys. **11**(1), 013021 (2009).